The Bowtie Effect in Cylindrical Waveguides

Antonio Astorino, Jesper Lægsgaard, and Karsten Rottwitt

***Abstract*—Modes in step-index fibers are often studied using a scalar model, born to the approximations allowed by the assumption of low refractive index contrast. Such approximations lead to a perfectly linear polarization in the resulting modes, among which the Bessel-like ones are attracting increasing interest for their many applications. These modes, as described by the scalar model, have a circularly symmetric irradiance. Nevertheless, in some cases, their symmetry disappears as their intensity profile exhibits angular ripples that cannot be foreseen by the scalar approach. In this paper, this effect is thoroughly analyzed.**

***Index Terms*—Bowtie effect, fiber modes, optical waveguides.**

I. Introduction

THE design of an optical fiber mainly aims at generating a refractive index profile such that the propagating field satisfies desired electromagnetic properties, depending on the application. For instance, single-mode fibers with special-purpose index profiles can be designed to reduce losses and modify the dispersion group-velocity dispersion (GVD) function [1]. In multimode fibers, graded index profiles have been introduced to reduce intermodal GVD [1], [2] and their parameters can be adjusted also to tailor non-linear effects [3].

Despite the existence of an infinite number of possible refractive index profiles, the analysis of modes in the simplifying case of ideal step-index fibers (SIFs) is extremely insightful. In fact, profile variations yield modes that, to a large extent, find equivalence (and strict similarity) with modes in SIFs, as long as the waveguide symmetry is cylindrical [4]. Even when the refractive index profile is very elaborate, the corresponding modes can often be approximated as those of SIFs [5]. Therefore, SIFs are a valid reference for mode analysis, classification, and notation.

The electromagnetic field (EMF) in SIFs can be described according to its vectorial nature, which gives rise to transverse electric (TE), transverse magnetic (TM), and hybrid (HE or EH) modes [6], [7]. Alternatively, due to the low refractive index difference between core and cladding, and supposing that the polarization of the modes is linear, the scalar approach is embraced [1], [8]. As a particular case, the scalar representation of the field in SIFs is very successful for its ability to accurately describe experimental results, where the so-called linearly polarized (LP) modes are excited with relatively simple techniques [9]. Nevertheless, with the recently increasing interest in higher-order Bessel-like modes, e.g. for amplification [10] and nonlinear processes [11]–[14], the LP approximation is insufficient. More specifically, as reported for the first time in [15], the circular symmetry of Bessel-like modes is broken when the mode order (i.e. the number of rings) increases sufficiently. Such an asymmetry, denoted *bowtie effect*, cannot be described by the scalar approach.

In this work, the conditions for the bowtie effect to occur are investigated, showing that the source of circular asymmetries in hybrid modes is found in the field angular dependence chosen when solving Maxwell's equations in cylindrical waveguides. The link between mathematical and experimental results is then provided, concluding that the circular asymmetry is an intrinsic property of all Bessel-like modes when excited with a linearly polarized source. Also, the bowtie effect is analytically described using SIFs as a model, and a parameter intended to quantify the phenomenon is suggested. Finally, for any cylindrical waveguide, a practical method to calculate the proposed parameter from intensity distribution measurements is illustrated.

This paper is organized as follows. Section II explores the source of the bowtie effect in any cylindrical waveguide by investigating the symmetries of guided modes. In Section III, the effect is deeply analyzed in case of SIFs and a characterization method is defined and extended to any cylindrical waveguide. Finally, the conclusions are presented in Section IV.

II. Mode Symmetries in Cylindrical Waveguides

A. Field Azimuthal Dependence

Considering a cylindrical waveguide whose longitudinal axis overlaps the z-axis of a cylindrical reference frame with coordinates r, ϕ, and z (radial, azimuthal, and longitudinal, respectively), separation of variables allows to write

$$\Psi(r,\phi,z,t) \propto R_\Psi(r)\Phi_\Psi(\phi)Z(z)T(t) \tag{1}$$

to represent, in a general form, any component of the electric field $[\mathbf{E} = (E_r, E_\phi, E_z)]$ and the magnetic field $[\mathbf{H} = (H_r, H_\phi, H_z)]$, at any time t. The radial and azimuthal functions may change, depending on the field component, as highlighted by the subscript Ψ $(= E_r, E_\phi, E_z, H_r, H_\phi, H_z)$. The functions $T(t)$ and $Z(z)$, instead, are the same for all components. They can be expressed as $\exp(i\omega t)$ and $\exp(-i\beta z)$, respectively, to obtain a wave traveling in the positive z-direction with unique propagation constant β, hence a *mode.*

The radial function $R_\Psi(r)$ is real valued and depends on the refractive index profile of the waveguide. As for the azimuthal

Manuscript received December 22, 2017; revised May 2, 2018; accepted May 24, 2018. Date of publication May 28, 2018; date of current version June 19, 2018. This work was supported by the European Union's Horizon 2020 research and innovation programme under the Marie Sklodowska-Curie grant agreement No. 642355. *(Corresponding author: Antonio Astorino.)*

The authors are with the DTU Fotonik, Ørsteds Plads, 2800 Kongens Lyngby, Denmark (e-mail: antonio.astorino.ing@gmail.com; jlag@fotonik.dtu.dk; karo@fotonik.dtu.dk).

Color versions of one or more of the figures in this paper are available online at http://ieeexplore.ieee.org.

Digital Object Identifier 10.1109/JLT.2018.2841409

dependency, instead, due to the symmetry of the system, $\Phi_\Psi(\phi)$ can be any periodic function with period 2π. Thus, with the additional assumptions that the Fourier theorem and superposition principle hold, $\Phi_\Psi(\phi)$ can be expressed as a sum of basis functions such that

$$\Phi_\Psi(\phi) = \sum_{\nu=-\infty}^{+\infty} \Phi_{\Psi,\nu} e^{i(\nu\phi)}, \quad \Phi_{\Psi,\nu} \in \mathbb{C} \tag{2}$$

where ν is called *azimuthal order* or *azimuthal mode number*. However, it can be shown that different values of $|\nu|$ yield different propagation constants, and hence, in general, a field obtained by substituting (2) into (1) is not a mode. As a consequence, only one harmonic of (2) at a time has to be considered to obtain a waveguide mode. Hence, $\Phi_\Psi(\phi)$ can be expressed by either a complex exponential function or a sinusoidal one.

It is clear that switching from exponential to cosine/sine representation is always allowed because the transformations involved are linear combinations of functions with the same $|\nu|$. Thus, the choice between the two options is completely arbitrary and not subject to any mathematical constraint. Despite that, hybrid modes obtained by choosing the exponential representation have different properties compared to those given by sinusoidal forms. These differences are crucial to this work, and hence both options are considered separately. Transverse modes, instead, are identical in both cases because they are obtained for $\nu = 0$, namely when the angular dependence disappears. Therefore, TE and TM modes are excluded from the analysis and mentioned only for completeness.

To distinguish the two detected options, the function Ψ is denoted with the subscripts "exp" and "cos", as follows.

$$\Psi^{\exp}(r,\phi,z,t) \propto R_\Psi(r) e^{i(\omega t - \beta z + \nu\phi)} \tag{3a}$$

or

$$\Psi^{\cos}(r,\phi,z,t) \propto R_\Psi(r) \cos(\nu\phi + \tilde{\phi}_\Psi) e^{i(\omega t - \beta z)} \tag{3b}$$

where $\tilde{\phi}_\Psi \in [0, 2\pi)$ is a constant to be determined.

B. Intensity Profile and Polarization

Assuming that R_{E_z} and R_{H_z} are known, and expressing the z-components of the EMF E_z and H_z as (3a) with proportionality constants Γ_e and Γ_h, respectively, the transverse field is completely defined by

$$E_r = \underbrace{\tau\Gamma_h \left(\beta \frac{\Gamma_e}{\Gamma_h} R'_{E_z} + i\nu\omega\mu_0 \frac{R_{H_z}}{r}\right)}_{\mathcal{E}_r(r)} e^{i\nu\phi} \tag{4a}$$

$$E_\phi = \underbrace{\tau\Gamma_h \left(i\nu\beta \frac{\Gamma_e}{\Gamma_h} \frac{R_{E_z}}{r} - \omega\mu_0 R'_{H_z}\right)}_{\mathcal{E}_\phi(r)} e^{i\nu\phi} \tag{4b}$$

$$H_r = \underbrace{\tau\Gamma_h \left(\beta R'_{H_z} - i\nu\omega\epsilon \frac{\Gamma_e}{\Gamma_h} \frac{R_{E_z}}{r}\right)}_{\mathcal{H}_r(r)} e^{i\nu\phi} \tag{4c}$$

$$H_\phi = \underbrace{\tau\Gamma_h \left(i\nu\beta \frac{R_{H_z}}{r} + \omega\epsilon \frac{\Gamma_e}{\Gamma_h} R'_{E_z}\right)}_{\mathcal{H}_\phi(r)} e^{i\nu\phi} \tag{4d}$$

where $\tau = -i/[\omega^2\mu_0\epsilon - \beta^2]$, μ_0 is the vacuum magnetic permeability, ϵ is the dielectric permittivity of the medium (dependent on r), and the prime symbol stands for the total derivative operator. The overall phase contribution given by $\exp[i(\omega t - \beta z)]$ is omitted for simplicity.

By denoting the complex conjugate with "*", the real part with $\Re\{\cdot\}$, the vector product with "$\wedge$", and the basis versor in the positive z-direction with $\hat{\boldsymbol{z}}$, the average intensity is

$$I = \frac{1}{2}\Re\left\{(\mathbf{E} \wedge \mathbf{H}^*)\hat{\boldsymbol{z}}\right\}. \tag{5}$$

For modes defined by (4), the field intensity becomes

$$I = \frac{1}{2}\Re\left\{\mathcal{E}_r(r)\mathcal{H}^*_\phi(r) - \mathcal{E}_\phi(r)\mathcal{H}^*_r(r)\right\} \tag{6}$$

which does not depend on ϕ. In addition, it is possible to prove that (4) describes a locally elliptically polarized (LEP) field by showing that the ratio Γ_e/Γ_h is purely imaginary (see Appendix IV), which entails that the r- and ϕ-components of $\mathbf{E}$ (or $\mathbf{H}$) are in quadrature. Due to this polarization property, modes obtained by using $\Psi^{\exp}$ are here named *LEP modes*.

If, instead, (3b) is selected to describe the longitudinal components of the field, it can be shown that the equation $|\tilde{\phi}_{E_z} - \tilde{\phi}_{H_z}| = \pi/2$ must be satisfied. Namely, the ϕ dependence of E_z must be in quadrature with that of H_z, in order to satisfy Maxwell's equations [8]. By choosing

$$E_z = \Gamma_e R_{E_z} \cos(\nu\phi + \tilde{\phi}) e^{i(\omega t - \beta z)} \tag{7a}$$

$$H_z = \Gamma_h R_{H_z} \sin(\nu\phi + \tilde{\phi}) e^{i(\omega t - \beta z)} \tag{7b}$$

with $\tilde{\phi}$ being an arbitrary constant, the transverse field becomes

$$E_r = \underbrace{\tau\Gamma_h \left(\beta \frac{\Gamma_e}{\Gamma_h} R'_{E_z} + \nu\omega\mu_0 \frac{R_{H_z}}{r}\right)}_{\mathcal{E}_r(r)} \cos(\nu\phi + \tilde{\phi}) \tag{8a}$$

$$E_\phi = \underbrace{\tau\Gamma_h \left(-\nu\beta \frac{\Gamma_e}{\Gamma_h} \frac{R_{E_z}}{r} - \omega\mu_0 R'_{H_z}\right)}_{\mathcal{E}_\phi(r)} \sin(\nu\phi + \tilde{\phi}) \tag{8b}$$

$$H_r = \underbrace{\tau\Gamma_h \left(\beta R'_{H_z} + \nu\omega\epsilon \frac{\Gamma_e}{\Gamma_h} \frac{R_{E_z}}{r}\right)}_{\mathcal{H}_r(r)} \sin(\nu\phi + \tilde{\phi}) \tag{8c}$$

$$H_\phi = \underbrace{\tau\Gamma_h \left(\nu\beta \frac{R_{H_z}}{r} + \omega\epsilon \frac{\Gamma_e}{\Gamma_h} R'_{E_z}\right)}_{\mathcal{H}_\phi(r)} \cos(\nu\phi + \tilde{\phi}) \tag{8d}$$

where, again, the dependence on t and z is omitted. Since the domain is invariant under rotation about the z-axis, any choice of $\tilde{\phi}$ determines an equivalent solution. Therefore, from now on, $\tilde{\phi}$ is set equal to zero, without loss of generality.

Defining $I_{r\phi}(r) = \mathcal{E}_r(r)\mathcal{H}^*_\phi(r)$ and $I_{\phi r}(r) = \mathcal{E}_\phi(r)\mathcal{H}^*_r(r)$, it is easy to see that, in this case, (5) becomes

$$\begin{aligned} I &= \frac{1}{2}\Re\left\{I_{r\phi}(r)\cos^2(\nu\phi) - I_{\phi r}(r)\sin^2(\nu\phi)\right\} \\ &= \frac{1}{4}\Re\left\{I_{r\phi}(r) - I_{\phi r}(r) + [I_{r\phi}(r) + I_{\phi r}(r)]\cos(2\nu\phi)\right\} \end{aligned} \tag{9}$$

which presents a sinusoidal dependence on ϕ. Such a dependence may be removed by designing a refractive index profile such that $I_{r\phi}(r) + I_{\phi r}(r) = 0$. However, this analysis is out of the scope of the present work, which focuses on the general cases where the above equality is not satisfied for all r.

By showing that the ratio Γ_e/Γ_h is real, in this case (see Appendix IV), it is easy to see that the transverse field is locally linearly polarized (LLP), meaning that, at any point, it oscillates over time along a straight line whose direction is not the same everywhere but is a function of the transverse coordinates. Hybrid modes obtained by using (3) are therefore called *LLP modes.*

C. The Source of the Bowtie Effect

As previously discussed, LEP modes have a circularly symmetric intensity profile. Such a symmetry has an intuitive justification. The field expressed by (4) is invariant under rotation, i.e. any variation in ϕ corresponds to a mere overall phase change. Also, any EMF component of LEP modes is proportional to $\exp[i(\omega t - \beta z + \nu\phi)]$, wherein it is clear that, for $\nu \neq 0$, a change in t is equivalent to a rotation about the z-axis, clockwise if $\nu > 0$ and counterclockwise if $\nu < 0$. Therefore, any circular asymmetry in the instantaneous intensity is averaged out by the time evolution of the mode.

Conversely, all LLP modes have circularly asymmetric intensity profile, oscillating along ϕ with period π/ν. This property is a consequence of the fact that the generating radial dependence $\Phi_\Psi(\phi) = \cos(\nu\phi + \tilde{\phi}_\Psi)$ is real, hence modulating the intensity profile with a behavior resembling the $\cos(2\nu\phi)$ function plus a vertical offset. This occurs independently of the refractive index profile, as long as it is a function of the radius only. When $|\nu| = 1$, this oscillation generates what has been denoted *bowtie effect* in Bessel-like modes, therefore named *bowtie modes* [15]. The generality of (9) ensures that the above conclusion applies to any cylindrical fiber. As a consequence, the azimuthal asymmetry of bowtie modes cannot be ascribed to a particular choice of index profile in a cylindrical waveguide, but only to the choice of Ψ, mathematically, or polarization, experimentally.

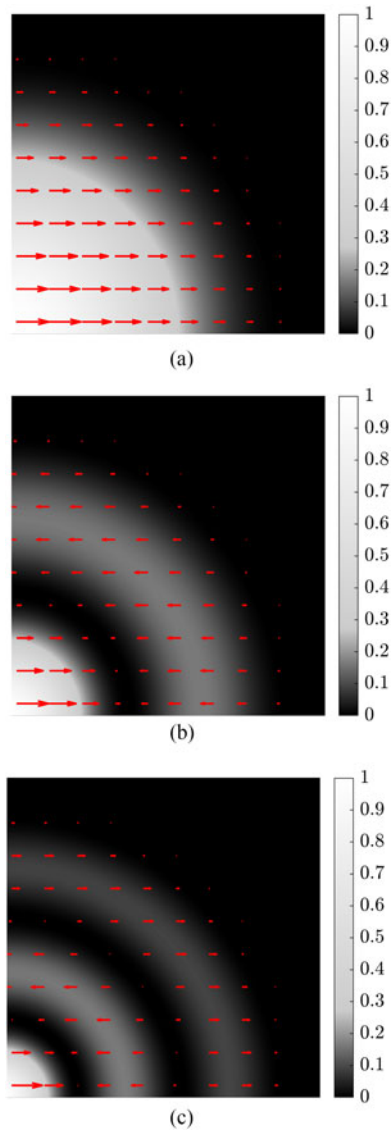

Fig. 1. Irradiance and transvers electric field vectors in the first quadrant of LLP (a) $HE_{1,1}$ (b) $HE_{1,2}$ and (c) $HE_{1,3}$ modes.

III. Analysis of Bowtie Modes

The conclusion drawn in Section II allows to state that the circular asymmetry of LLP modes is a direct consequence of the lack of polarization symmetry imposed by a non-rotating (and circularly asymmetric) vector field. In other words, in a perfectly cylindrical medium, there is no reason for the propagating modes not to have the same symmetry, unless the polarization of the field used to excite a given mode is not invariant under rotation around the fiber axis, in which case the symmetry is automatically broken.

If true, the last observation should also be in agreement with the definition of $LP_{l,m}$ modes, according to which the intensity profile has $2l$ zeros along ϕ and m maxima along r [1]. Following the above line of reasoning, since the field of any $LP_{l,m}$ mode is not invariant under rotation, the intensity has to exhibit circular asymmetry. However, this statement is contradicted by the case $l = 0$. In fact, the intensity profile of $LP_{0,m}$ modes, also known as Bessel-like modes, is circularly symmetric, in theory. Nevertheless, this contradiction is only apparent and due to the approximations made to calculate LP modes, based on a scalar approach. In order to capture the azimuthal asymmetry of Bessel-like modes, the analysis requires a full-vectorial framework, wherein such modes correspond to LLP $HE_{1,\mu}$ modes, μ being the *mode rank* [16], also called *radial mode number* [8].

Three LLP $HE_{1,\mu}$ modes are depicted in Fig. 1 as an example. The characteristic that makes them unique among full vectorial modes is their approximately linearly polarized $\mathbf{E}_\perp$, enabling them to be easily generated with a linearly polarized source [17]. This is an obvious advantage, from the experimental point of view. However, the similarity of LLP $HE_{1,\mu}$ with $LP_{0,m}$ modes can be misleading. In fact, it might be concluded that the vectorial nature of $HE_{1,\mu}$ modes can be neglected because their corresponding scalar description, which is linearly polarized, is a very good approximation. The bowtie effect proves the opposite.

A. Modes in Step-Index Fibers

For further investigation on the bowtie effect, SIFs are considered as a model. From now on, the subscripts "0," "co," and "cl" are used to indicate vacuum, core, and cladding, respectively, whereas the subscript j $(= 0, \mathrm{co}, \mathrm{cl})$ is used when the medium is not specified. Following this notation,

- $n_j = \sqrt{\epsilon_j/\epsilon_0}$ is refractive index
- $k_j = \omega\sqrt{\mu_0\epsilon_j}$ is the wave number
- λ_0 is the wavelength in free space
- $\Delta = (n_{\mathrm{co}}^2 - n_{\mathrm{cl}}^2)/(2n_{\mathrm{co}}^2)$ is the refractive index contrast

By taking the curl of Maxwell's curl equations, any EMF component [given by (1)] in each medium of a SIF satisfies

$$\nabla^2\Psi - \epsilon_j\mu_0\frac{\partial^2\Psi}{\partial t^2} = 0. \tag{10}$$

Defining the real quantities $u = \sqrt{k_{\mathrm{co}}^2 - \beta^2}$ and $w = \sqrt{\beta^2 - k_{\mathrm{cl}}^2}$, either $\Psi^{\exp}$ or $\Psi^{\cos}$ yields a radial dependence equal to the Bessel's function of the first kind $J_\nu(ur)$, inside the core, and the modified Bessel's functions of the second kind $K_\nu(wr)$, in the cladding, both of the νth order. The equations describing LEP and LLP modes in SIFs are reported in Appendix B, along with the definition of the P-parameter, which plays an essential role in the analysis of the bowtie effect. This parameter was first introduced in [16] to distinguish between HE and EH modes under the weakly guiding approximation, which entails that the $P \approx \pm 1$. For purely historical reasons (not reported for brevity), $P \approx -1$ indicates HE modes and $P \approx +1$ indicates EH modes. Here, this classification is generalized by denoting with HE or EH all modes for which $P < 0$ or $P > 0$, respectively.

B. Qualitative Analysis of the Bowtie Effect in SIFs

In the following, LLP $\mathrm{HE}_{1,\mu}$ modes are considered. The intensity of such modes is explicitly calculated by substituting (20) in (5), for $|\nu| = 1$. In particular, let $I_{\mathrm{co,const}}^{\mathrm{LLP}}$ represent the part of I invariant with respect to changes of ϕ and $I_{\mathrm{co,osc}}^{\mathrm{LLP}}$ be the part depending on ϕ, as follows (a step-by-step demonstration is reported in Appendix C).

$$I_{\mathrm{co,const}}^{\mathrm{LLP}} = \frac{\omega\beta\mu_0|C|^2}{8u^2}\left[\left(1 + \frac{n_{\mathrm{co}}^2}{n_{\mathrm{eff}}^2P^2}\right)\left(J_0^2 + J_2^2\right) - \frac{1}{P}\left(1 + \frac{n_{\mathrm{co}}^2}{n_{\mathrm{eff}}^2}\right)\left(J_0^2 - J_2^2\right)\right] \tag{11a}$$

$$I_{\mathrm{co,osc}}^{\mathrm{LLP}} = \frac{\omega\beta\mu_0|C|^2}{8u^2}\left(1 - \frac{n_{\mathrm{co}}^2}{n_{\mathrm{eff}}^2P^2}\right)2J_0J_2\cos(2\phi) \tag{11b}$$

where n_{eff} is defined as β/k_0.

For a quantitative evaluation of the bowtie effect, (11a) and (11b) should now be compared against each other. However, such a comparison is not straightforward due to the presence of several radial trends. Therefore, some simplifying approximations are needed before proceeding with the analysis. In particular, it can be observed that (11a) contains a negative term, namely

$$\frac{\omega\beta\mu_0|C|^2}{8u^2}\frac{1}{P}\left(1 + \frac{n_{\mathrm{co}}^2}{n_{\mathrm{eff}}^2}\right)J_2^2 \tag{12}$$

Notice that indeed (12) is negative because $P < 0$ by definition of HE modes. This term can be compared with a positive one in (11a) having the same radial dependence, namely

$$\frac{\omega\beta\mu_0|C|^2}{8u^2}\left(1 + \frac{n_{\mathrm{co}}^2}{n_{\mathrm{eff}}^2P^2}\right)J_2^2 \tag{13}$$

It is clear that, under the assumption $P \approx -1$, (12) and (13) almost cancel out, meaning that their combined contribution to (11a) can be neglected in case of small refractive index contrast. Similarly, the two terms in (11a) depending on J_0^2 can be merged into one, as they give a positive contribution with approximately the same magnitude. As a result

$$I_{\mathrm{co}}^{\mathrm{LLP}} \approx \underbrace{\frac{\omega\beta\mu_0|C|^2}{4u^2}\left(1 + \frac{n_{\mathrm{co}}^2}{n_{\mathrm{eff}}^2P^2}\right)J_0^2}_{=\tilde{I}_{\mathrm{co,const}}^{\mathrm{LLP}}} + \underbrace{\frac{\omega\beta\mu_0|C|^2}{4u^2}\left(1 - \frac{n_{\mathrm{co}}^2}{n_{\mathrm{eff}}^2P^2}\right)J_0J_2\cos(2\phi)}_{=I_{\mathrm{co,osc}}^{\mathrm{LLP}}} \tag{14}$$

which reduces the analysis to a comparison between two terms only. Notice the tilde symbol on $\tilde{I}_{\mathrm{co,const}}^{\mathrm{LLP}}$ used to make this term distinguishable from its exact version. The comparison should be done for all values of $r \leq a$, because the two remaining terms still have different radial dependence. Despite that, since both J_0^2 and $J_0J_2\cos(2\phi)$ functions are bounded, an insightful result is obtained by analyzing the magnitude of the ratio between only the coefficients in (14), namely

$$\left|\frac{\frac{\omega\beta\mu_0|C|^2}{4u^2}\left(1 - \frac{n_{\mathrm{co}}^2}{n_{\mathrm{eff}}^2P^2}\right)}{\frac{\omega\beta\mu_0|C|^2}{4u^2}\left(1 + \frac{n_{\mathrm{co}}^2}{n_{\mathrm{eff}}^2P^2}\right)}\right| = \left|\frac{\left(n_{\mathrm{eff}}^2P^2 - n_{\mathrm{co}}^2\right)}{\left(n_{\mathrm{eff}}^2P^2 + n_{\mathrm{co}}^2\right)}\right| \approx \frac{\left(n_{\mathrm{co}}^2 - n_{\mathrm{eff}}^2\right)}{\left(n_{\mathrm{co}}^2 + n_{\mathrm{eff}}^2\right)} \tag{15}$$

where the last approximation is due to the assumption $P^2 \approx 1$ and the norm function has been removed because of the known property $n_{\mathrm{eff}}^2 < n_{\mathrm{co}}^2$. It is important to highlight that a small refractive index contrast does not ensure the validity of the approximation adopted for P, as large core radii allow values of $|P|$ significantly different from unity.

Qualitatively, (15) shows that higher values of n_{eff}, i.e. those close to n_{co}, imply lower magnitude of the oscillating term, compared to that of the constant term. In particular, (15) tends to 0 as n_{eff} approaches n_{co}. In terms of radial mode numbers, and remembering that the lower the rank the higher n_{eff}, if $\mu = 1$ the bowtie effect is minimized. Conversely, when n_{eff} is sufficiently low, hence for higher values of μ, (15) increases, allowing the bowtie effect to surface, thus confirming what was found experimentally in [15].

The adopted approximations can be further validated by showing that the rings of $I_{\mathrm{co,osc}}^{\mathrm{LLP}}$ overlap those of $\tilde{I}_{\mathrm{co,const}}^{\mathrm{LLP}}$. To do so, the radial dependence of both functions is depicted in Fig. 2, which shows that the sought overlapping exists and allows to extrapolate a few more general details about the phenomenon. First, the absolute extrema of both parts decay with similar trends, ensuring that all the rings are affected by $I_{\mathrm{co,osc}}^{\mathrm{LLP}}$ with roughly the same magnitude. Second, $I_{\mathrm{co,osc}}^{\mathrm{LLP}}$ is very weak

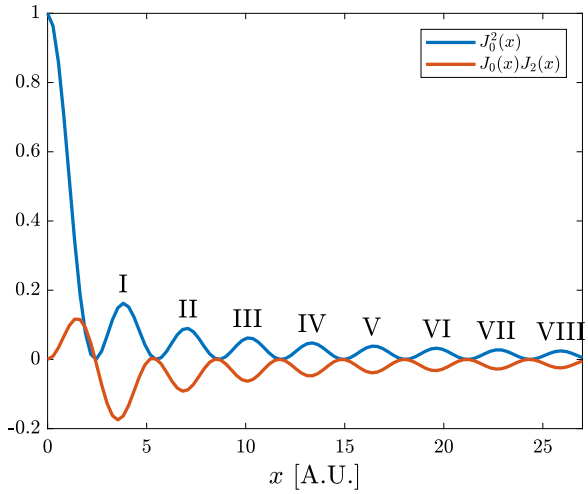

Fig. 2. Radial dependence of $\tilde{I}^{\mathrm{LLP}}_{\mathrm{co,const}}$ and $I^{\mathrm{LLP}}_{\mathrm{co,osc}}$. The Roman numerals represent the ring numbers, counted from the mode center outwards, corresponding to the peaks of the functions.

in the central spot, where instead $\tilde{I}^{\mathrm{LLP}}_{\mathrm{co,const}}$ is predominant, which entails that the bowtie effect is more evident in the rings than in proximity of the center. Last, since the LLP $\mathrm{HE}_{1,1}$ mode has no rings, a very low asymmetry is guaranteed by a low refractive index contrast.

C. Characterization of Bowtie Modes

The analysis developed so far is extremely sensitive to the value of P, which varies with n_{eff} and, therefore, with μ. Hence, the approximation $P = \pm 1$ and the resultant equations must be considered only for the sake of a qualitative description of the bowtie effect.

For a more accurate characterization of the phenomenon not affected by any approximation, hence involving the exact quantities defined in (11), the following parameter is proposed.

$$M_{\mathrm{BT}} = \frac{\max\limits_{r,\phi}\left\{\left|I^{\mathrm{LLP}}_{\mathrm{co,osc}}\right|\right\}}{\max\limits_{r}\left\{I^{\mathrm{LLP}}_{\mathrm{co,const}}\right\}} \tag{16}$$

Such a parameter allows to evaluate the distortion due to the bowtie effect. As an example, three simulated bowtie modes are shown in Fig. 3. The exposure of the images has been increased to emphasize the effect. For each bowtie mode, the parameter M_{BT} is also displayed. As predicted by (15), the bowtie shape looks more pronounced for $\mu = 7$ than $\mu = 4$, whereas it is basically imperceptible when $\mu = 1$, as confirmed by the corresponding M_{BT}.

In some cases, the trend of M_{BT} with respect to μ goes against the deductions made by analyzing (15). To show this, M_{BT} is plotted as a function of Δ in Fig. 4, where $\lambda_0 = 1550\,\mathrm{nm}$, $a = 6.8\,\mu\mathrm{m}$, $n_{\mathrm{co}} = 1.45$ and n_{cl} sweeps from 1.45 to 1.00. It is interesting to see that the prediction of (15) is often violated by the mode with the highest rank. Especially when such a mode is very close to its cut-off frequency, corresponding to the steepest part of the M_{BT} vs. Δ curve, M_{BT} tends to zero. By moving away from the cut-off frequency, the effect rapidly

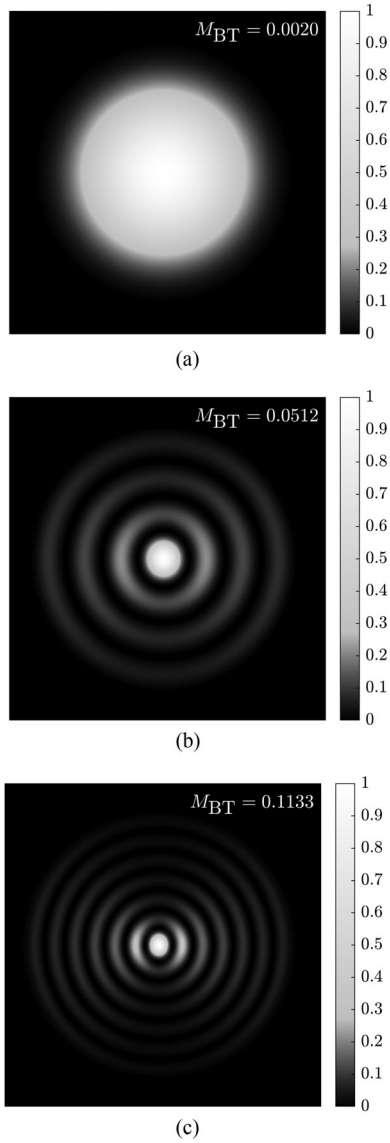

Fig. 3. Intensity profile of LLP (a) $\mathrm{HE}_{1,1}$ (b) $\mathrm{HE}_{1,4}$ and (c) $\mathrm{HE}_{1,7}$ modes for a fiber with parameters $a = 7\,\mu\mathrm{m}$, $n_{\mathrm{co}} = 1.45$, $n_{\mathrm{cl}} = 1.35$, at $\lambda_0 = 850\,\mathrm{nm}$.

increases. As an example, with reference to Fig. 4, the intensity profile of the LLP $\mathrm{HE}_{1,8}$ mode is shown in Fig. 5(a) and (b), for $\Delta = 0.163$ and $\Delta = 0.167$, respectively. In the first case, very close to cut-off frequency, $M_{\mathrm{BT}} \approx 0.0448$ whereas, in the second, $M_{\mathrm{BT}} \approx 0.1049$. This behavior is in agreement with the fact that Bessel-like modes spread in the cladding over a large area, when close to cut-off [6]. Since the bowtie effect is a vectorial effect, not seen in the scalar approximation, it is expected to vanish if the field strength at the core-cladding interface in a step-index fiber is negligible. This is the case at cut-off.

Another insightful analysis can be conducted by evaluating the dependence of the bowtie effect with respect to the wavelength and the core size. However, it turns out that if the ratio a/λ_0 is constant, a change in both parameters does not affect M_{BT}. Therefore, it is convenient to define the *normalized core diameter* as $\tilde{d} = 2a/\lambda_0$ and show M_{BT} as a function of $\tilde{d}$. An example is depicted in Fig. 6, where a fiber with $n_{\mathrm{co}} = 1.45$

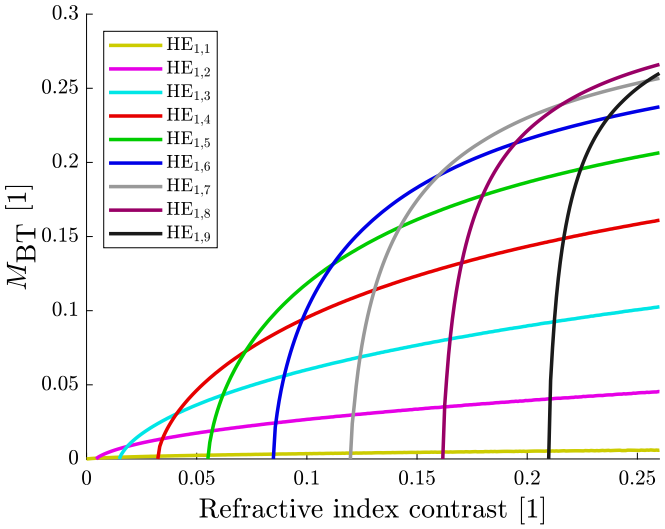

Fig. 4. M_{BT} as a function of Δ for a SIF with $a = 6.8\,\mu$m, $n_{\mathrm{co}} = 1.45$, at $\lambda_0 = 1550\,$nm.

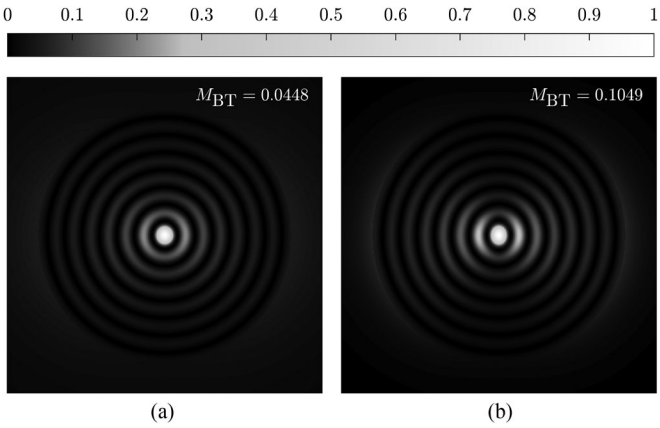

Fig. 5. Intensity profile of the LLP $\mathrm{HE}_{1,8}$ mode in a SIF with $a = 6.8\,\mu$m, $n_{\mathrm{co}} = 1.45$, at $\lambda_0 = 1550\,$nm, for (a) $\Delta = 0.163$ and (b) $\Delta = 0.167$.

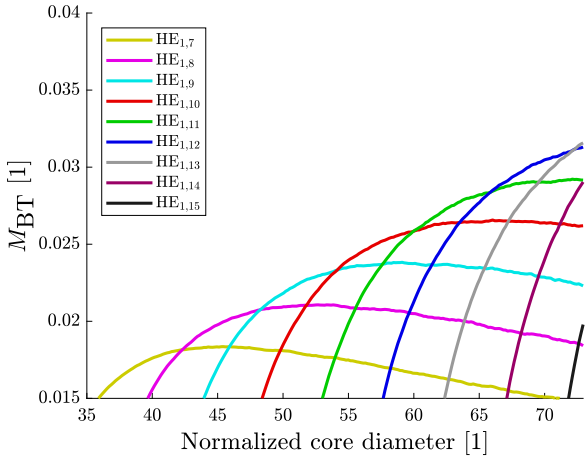

Fig. 6. M_{BT} as a function of $\tilde{d}$ for $n_{\mathrm{co}} = 1.45$ and $\Delta = 0.01$.

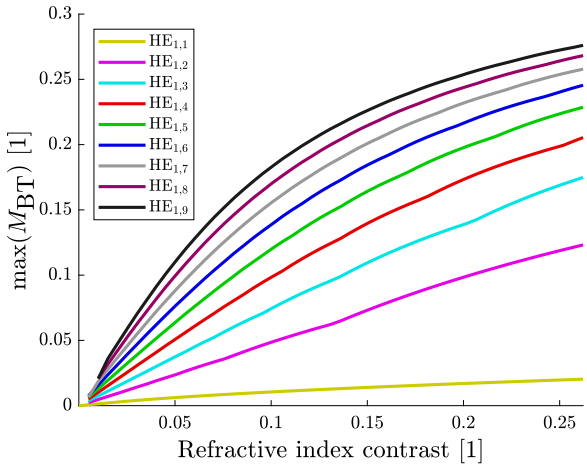

Fig. 7. Maximum M_{BT} as a function of the Δ for $n_{\mathrm{co}} = 1.45$ and $\mu = 1, 2, \ldots, 9$.

and $\Delta = 0.01$ is considered. The plot confirms that modes with higher rank can reach larger values of M_{BT}. However, a low Δ ensures a very low bowtie effect. In this example, to achieve only $M_{\mathrm{BT}} \approx 0.0320$, $\tilde{d} \approx 73$ is needed, which corresponds to a diameter of about 62 μm at $\lambda_0 = 850$ nm. The weak bowtie effect obtained in case of low Δ is obviously due to small difference in the boundary conditions experienced by the electric field orthogonal and tangential to the core-cladding interface, which makes the medium more homogeneous to the field.

As observed in Fig. 6, the bowtie effect has a global maximum when considered as a function of $\tilde{d}$, hence for a fixed Δ. On the other hand, Fig. 4 suggests that such a maximum increases with Δ. To see this, the maximum M_{BT} as a function of Δ is depicted in Fig. 7, for $\mu = 1, 2, \ldots, 9$. In Fig. 8, M_{BT} is plotted against both $\tilde{d}$ and Δ for $\mu = 7$, as an example.

D. Measuring the Bowtie Effect

Although the characterization of bowtie modes has been developed using SIFs as a model, it can be easily extended to any cylindrical waveguide. In fact, for practical use, M_{BT} can be calculated from the image displaying the irradiance of a bowtie mode, independently of the refractive index profile of the waveguide in which the mode is formed. If such a picture is available the following steps can be followed to estimate M_{BT}.

1) Find the global maximum of the intensity and use it as the denominator in (16)
2) Rotate the image through 90° about the position of the maximum intensity (i.e. the mode center)
3) Subtract the obtained image from the original one to obtain $I^{\mathrm{LLP}}_{\mathrm{co,osc}}$
4) Find the maximum of $I^{\mathrm{LLP}}_{\mathrm{co,osc}}$ and use it as the numerator of (16)
5) Calculate M_{BT} through (16)

The reliability of the proposed algorithm depends on the quality of the image. In particular, it is important that the image sensor used to capture the irradiance has a linear response to the intensity of the light impinging on it. Plotting the calculated oscillating term obtained at step 3 might be helpful to determine the quality of the original image in terms of symmetries.

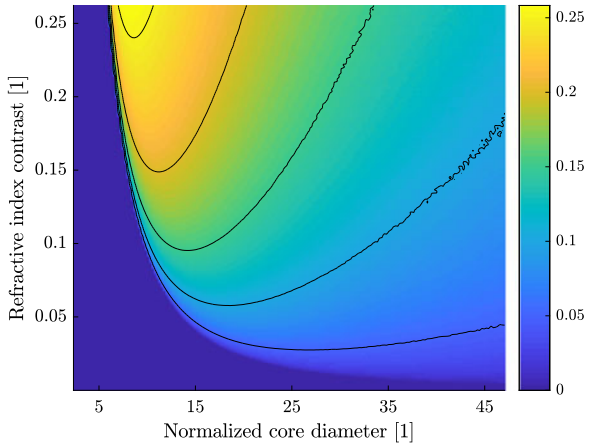

Fig. 8. M_{BT} as a function of the $\tilde{d}$ and Δ for $n_{\mathrm{co}} = 1.45$ and $\mu = 7$.

IV. Conclusion

In this paper, the circular asymmetry affecting Bessel-like modes in cylindrical waveguides has been studied.

To accomplish this task, full-vectorial fiber modes have been analyzed using step-index fibers (SIFs) as a model. The focus has been on the differences between two possible sets of hybrid modes, here denoted locally elliptically polarized (LEP) and locally linearly polarized (LLP) modes. In particular, it has been shown that the field distribution of LEP modes is invariant under rotation, whereas that of LLP modes is not. In addition, it has been demonstrated that all hybrid modes are circularly asymmetric in their LLP representation and symmetric in their LEP version, suggesting that the field invariance under rotation is a necessary and sufficient condition for the intensity of any guided mode to be circularly symmetric.

In the particular case of Bessel-like modes, when a linearly polarized beam is used as a source for mode excitation, LLP modes are easily generated. The consequent azimuthal asymmetry, denoted *bowtie effect,* has been analyzed in detail. For this purpose, the parameter M_{BT} has been defined to quantify the bowtie effect. The trend of M_{BT} as a function of the refractive index contrast (Δ) and the core diameter normalized with respect to the wavelength ($\tilde{d}$) has been graphically studied, showing that M_{BT} always increases with Δ, whereas it is a concave function of $\tilde{d}$.

Finally, a method to compute M_{BT} from the measured intensity profile of a given Bessel-like mode in any cylindrical waveguide has been proposed.

Appendix A
Phase Relation Between Γ_e and Γ_h

From Maxwell's equation $\nabla \mathbf{D} = 0$, where $\mathbf{D} = \epsilon \mathbf{E}$, it immediately follows that, in cylindrical coordinates,

$$\frac{1}{r}\frac{\partial (rE_r)}{\partial r} + \frac{1}{r}\frac{\partial E_\phi}{\partial \phi} - i\beta E_z + \frac{\epsilon'}{\epsilon}E_r = 0. \tag{17}$$

Substituting (4) in (17) gives

$$\frac{\Gamma_e}{\Gamma_h}\left[\frac{\left(r\tau R'_{E_z}\right)'}{r} - \nu^2\frac{\tau R_{E_z}}{r^2} - iR_{E_z} + \frac{\epsilon'\tau R'_{E_z}}{\epsilon}\right] = \frac{-i\nu\omega\mu_0}{\beta r}\left[\left(\tau R_{H_z}\right)' - \tau R'_{H_z} + \frac{\epsilon'\tau R_{H_z}}{\epsilon}\right]. \tag{18}$$

Since the terms in square brackets are purely imaginary (as τ), when the exponential function is used for the angular dependence of the EMF, the ratio between Γ_e and Γ_h is also purely imaginary.

Similarly, substituting (8) in (17) yields the same relation as (18) with the sole difference that the imaginary unit multiplying the right-hand side is missing. This makes the ratio Γ_e/Γ_h real, in case the azimuthal dependence of the EMF is sinusoidal.

Appendix B
LEP and LLP Mode Equations

Omitting the overall phase contribution given by $\exp[i(\omega t - \beta z)]$, the EMF can be written in the following forms.

For LEP modes, in the core,

$$E_{r,\mathrm{co}} = \left(\frac{\omega\mu_0\nu}{u^2}\frac{J_\nu(ur)}{r}C - i\frac{\beta}{u}J'_\nu(ur)A\right)e^{i\nu\phi} \tag{19a}$$

$$E_{\phi,\mathrm{co}} = \left(\frac{\beta\nu}{u^2}\frac{J_\nu(ur)}{r}A + i\frac{\omega\mu_0}{u}J'_\nu(ur)C\right)e^{i\nu\phi} \tag{19b}$$

$$E_{z,\mathrm{co}} = AJ_\nu(ur)e^{i\nu\phi} \tag{19c}$$

$$H_{r,\mathrm{co}} = \left(-\frac{\omega\epsilon_{\mathrm{co}}\nu}{u^2}\frac{J_\nu(ur)}{r}A - i\frac{\beta}{u}J'_\nu(ur)C\right)e^{i\nu\phi} \tag{19d}$$

$$H_{\phi,\mathrm{co}} = \left(\frac{\beta\nu}{u^2}\frac{J_\nu(ur)}{r}C - i\frac{\omega\epsilon_{\mathrm{co}}}{u}J'_\nu(ur)A\right)e^{i\nu\phi} \tag{19e}$$

$$H_{z,\mathrm{co}} = CJ_\nu(ur)e^{i\nu\phi} \tag{19f}$$

and, in the cladding,

$$E_{r,\mathrm{cl}} = \left(-\frac{\omega\mu_0\nu}{w^2}\frac{K_\nu(wr)}{r}D + i\frac{\beta}{w}K'_\nu(wr)B\right)e^{i\nu\phi} \tag{19g}$$

$$E_{\phi,\mathrm{cl}} = \left(-\frac{\beta\nu}{w^2}\frac{K_\nu(wr)}{r}B - i\frac{\omega\mu_0}{w}K'_\nu(wr)D\right)e^{i\nu\phi} \tag{19h}$$

$$E_{z,\mathrm{cl}} = BK_\nu(wr)e^{i\nu\phi} \tag{19i}$$

$$H_{r,\mathrm{cl}} = \left(\frac{\omega\epsilon_2\nu}{w^2}\frac{K_\nu(wr)}{r}B + i\frac{\beta}{w}K'_\nu(wr)D\right)e^{i\nu\phi} \tag{19j}$$

$$H_{\phi,\mathrm{cl}} = \left(-\frac{\beta\nu}{w^2}\frac{K_\nu(wr)}{r}D + i\frac{\omega\epsilon_2}{w}K'_\nu(wr)B\right)e^{i\nu\phi} \tag{19k}$$

$$H_{z,\mathrm{cl}} = DK_\nu(wr)e^{i\nu\phi}. \tag{19l}$$

In case of LLP modes, in the core,

$$E_{r,\mathrm{co}} = \left(\frac{\omega\mu_0\nu}{u^2}\frac{J_\nu(ur)}{r}C - i\frac{\beta}{u}J'_\nu(ur)A\right)\cos(\nu\phi) \quad (20a)$$

$$E_{\phi,\mathrm{co}} = \left(i\frac{\beta\nu}{u^2}\frac{J_\nu(ur)}{r}A - \frac{\omega\mu_0}{u}J'_\nu(ur)C\right)\sin(\nu\phi) \quad (20b)$$

$$E_{z,\mathrm{co}} = AJ_\nu(ur)\cos(\nu\phi) \quad (20c)$$

$$H_{r,\mathrm{co}} = \left(-i\frac{\omega\epsilon_{\mathrm{co}}\nu}{u^2}\frac{J_\nu(ur)}{r}A + \frac{\beta}{u}J'_\nu(ur)C\right)\sin(\nu\phi) \quad (20d)$$

$$H_{\phi,\mathrm{co}} = \left(\frac{\beta\nu}{u^2}\frac{J_\nu(ur)}{r}C - i\frac{\omega\epsilon_{\mathrm{co}}}{u}J'_\nu(ur)A\right)\cos(\nu\phi) \quad (20e)$$

$$H_{z,\mathrm{co}} = iCJ_\nu(ur)\sin(\nu\phi) \quad (20f)$$

and, in the cladding,

$$E_{r,\mathrm{cl}} = \left(-\frac{\omega\mu_0\nu}{w^2}\frac{K_\nu(wr)}{r}D + i\frac{\beta}{w}K'_\nu(wr)B\right)\cos(\nu\phi) \quad (20g)$$

$$E_{\phi,\mathrm{cl}} = \left(-i\frac{\beta\nu}{w^2}\frac{K_\nu(wr)}{r}B + \frac{\omega\mu_0}{w}K'_\nu(wr)D\right)\sin(\nu\phi) \quad (20h)$$

$$E_{z,\mathrm{cl}} = BK_\nu(wr)\cos(\nu\phi) \quad (20i)$$

$$H_{r,\mathrm{cl}} = \left(i\frac{\omega\epsilon_2\nu}{w^2}\frac{K_\nu(wr)}{r}B - \frac{\beta}{w}K'_\nu(wr)D\right)\sin(\nu\phi) \quad (20j)$$

$$H_{\phi,\mathrm{cl}} = \left(-\frac{\beta\nu}{w^2}\frac{K_\nu(wr)}{r}D + i\frac{\omega\epsilon_2}{w}K'_\nu(wr)B\right)\cos(\nu\phi) \quad (20k)$$

$$H_{z,\mathrm{cl}} = iDK_\nu(wr)\sin(\nu\phi). \quad (20l)$$

At the core-cladding interface, the boundary conditions allow to calculate A, B, D, and β, whereas C is left as a free parameter. Excluding the cases of TE and TM modes, the following relations hold.

$$D = \frac{CJ_\nu(ua)}{K_\nu(wa)} \quad (21a)$$

$$A = -i\frac{\omega\mu_0|\nu|C}{\beta\nu}\frac{1}{P} \quad (21b)$$

$$B = -i\frac{\omega\mu_0|\nu|D}{\beta\nu}\frac{1}{P} \quad (21c)$$

where a is the core radius and P is given by

$$P = \frac{\frac{|\nu|}{a}\left(\frac{1}{u^2}+\frac{1}{w^2}\right)}{\frac{1}{u}\frac{J'_\nu(ua)}{J_\nu(ua)}+\frac{1}{w}\frac{K'_\nu(wa)}{K_\nu(wa)}}. \quad (22)$$

Appendix C
Derivation of (11)

According to (5), the intensity of any LLP mode inside the core is

$$I_{\mathrm{co}}^{\mathrm{LLP}} = \frac{1}{2}\Re\{E_{r,\mathrm{co}}H^*_{\phi,\mathrm{co}} - E_{\phi,\mathrm{co}}H^*_{r,\mathrm{co}}\} \quad (23)$$

where the field components are given in (20). Let

$$R_A = \frac{\nu}{u^2}\frac{J_\nu(ur)}{r} \quad (24a)$$

$$R_B = \frac{J'_\nu(ur)}{u} \quad (24b)$$

so that (23) can be written as

$$\begin{aligned} I_{\mathrm{co}}^{\mathrm{LLP}} &= \frac{1}{2}\Re\{(\omega\mu_0 R_A C - i\beta R_B A)(\beta R_A C^* + i\omega\epsilon_{\mathrm{co}} R_B A^*) \\ &\quad \cdot\cos^2(\nu\phi) \\ &\quad -(i\beta R_A A - \omega\mu_0 R_B C)(i\omega\epsilon_{\mathrm{co}} R_A A^* + \beta R_B C^*) \\ &\quad \cdot\sin^2(\nu\phi)\} \\ &= \frac{1}{2}\Re\Big\{(\omega\mu_0\beta R_A^2|C|^2 + ik_{\mathrm{co}}^2 R_A R_B A^* C \\ &\quad -i\beta^2 R_A R_B AC^* + \omega\epsilon_{\mathrm{co}}\beta R_B^2|A|^2)\cos^2(\nu\phi) \\ &\quad -(-\omega\epsilon_{\mathrm{co}}\beta R_A^2|A|^2 + i\beta^2 R_A R_B AC^* \\ &\quad -ik_{\mathrm{co}}^2 R_A R_B A^* C - \omega\mu_0\beta R_B^2|C|^2)\sin^2(\nu\phi)\Big\} \\ &= \frac{1}{2}\Re\Big\{\omega\mu_0\beta|C|^2\left[R_A^2\cos^2(\nu\phi) + R_B^2\sin^2(\nu\phi)\right] \\ &\quad +\omega\epsilon_{\mathrm{co}}\beta|A|^2\left[R_B^2\cos^2(\nu\phi) + R_A^2\sin^2(\nu\phi)\right] \\ &\quad +ik_{\mathrm{co}}^2 R_A R_B A^* C - i\beta^2 R_A R_B AC^*\Big\}. \end{aligned} \quad (25)$$

Using (21b), the last result becomes

$$\begin{aligned} I_{\mathrm{co}}^{\mathrm{LLP}} &= \frac{\omega\mu_0|C|^2}{2\beta}\Big\{\beta^2\left[R_A^2\cos^2(\nu\phi) + R_B^2\sin^2(\nu\phi)\right] \\ &\quad +\frac{k_{\mathrm{co}}^2}{P^2}\left[R_B^2\cos^2(\nu\phi) + R_A^2\sin^2(\nu\phi)\right] \\ &\quad -\frac{|\nu|}{\nu P}(k_{\mathrm{co}}^2+\beta^2)R_A R_B\Big\}. \end{aligned} \quad (26)$$

The properties

$$J'_\nu(x) = \frac{1}{2}[J_{\nu-1}(x) - J_{\nu+1}(x)] \quad (27a)$$

$$\frac{J_\nu(x)}{x} = \frac{1}{2\nu}[J_{\nu-1}(x) + J_{\nu+1}(x)] \quad (27b)$$

allow to write

$$R_A = \frac{1}{2u}[J_{\nu-1}(ur) + J_{\nu+1}(ur)] \quad (28a)$$

$$R_B = \frac{1}{2u}[J_{\nu-1}(ur) - J_{\nu+1}(ur)] \quad (28b)$$

from which it follows that

$$R_A^2 = \frac{1}{4u^2}[J_{\nu-1}^2 + J_{\nu+1}^2 + 2J_{\nu-1}J_{\nu+1}] \tag{29a}$$

$$R_B^2 = \frac{1}{4u^2}[J_{\nu-1}^2 + J_{\nu+1}^2 - 2J_{\nu-1}J_{\nu+1}] \tag{29b}$$

$$R_A R_B = \frac{1}{4u^2}[J_{\nu-1}^2 - J_{\nu+1}^2] \tag{29c}$$

where the dependence on ur has been omitted for brevity. Substituting (29) in (25) and k_{co}^2/β^2 with $n_{\text{co}}^2/n_{\text{eff}}^2$ yields

$$\begin{aligned} I_{\text{co}}^{\text{LLP}} = {} & \frac{\omega\mu_0\beta|C|^2}{8u^2} \\ & \cdot \Bigg(\big\{ J_{\nu-1}^2 + J_{\nu+1}^2 \\ & + 2J_{\nu-1}J_{\nu+1}\left[\cos^2(\nu\phi) - \sin^2(\nu\phi)\right] \big\} \\ & + \frac{n_{\text{co}}^2}{n_{\text{eff}}^2 P^2}\big\{ J_{\nu-1}^2 + J_{\nu+1}^2 \\ & - 2J_{\nu-1}J_{\nu+1}\left[\cos^2(\nu\phi) - \sin^2(\nu\phi)\right] \big\} \\ & - \frac{|\nu|}{\nu P}\left(1 + \frac{n_{\text{co}}^2}{n_{\text{eff}}^2}\right)\left(J_{\nu-1}^2 - J_{\nu+1}^2\right) \Bigg) \end{aligned} \tag{30}$$

Using the trigonometric identities $\cos^2(x) = [1 + \cos(2x)]/2$ and $\sin^2(x) = [1 - \cos(2x)]/2$, the last expression becomes

$$\begin{aligned} I_{\text{co}}^{\text{LLP}} = {} & \frac{\omega\beta\mu_0|C|^2}{8u^2} \\ & \cdot \Bigg[\left(1 + \frac{n_{\text{co}}^2}{n_{\text{eff}}^2 P^2}\right)\left(J_{\nu-1}^2 + J_{\nu+1}^2\right) + \\ & - \frac{|\nu|}{\nu P}\left(1 + \frac{n_{\text{co}}^2}{n_{\text{eff}}^2}\right)\left(J_{\nu-1}^2 - J_{\nu+1}^2\right) \\ & + \left(1 - \frac{n_{\text{co}}^2}{n_{\text{eff}}^2 P^2}\right) 2J_{\nu-1}J_{\nu+1}\cos(2\nu\phi) \Bigg] \end{aligned} \tag{31}$$

which leads to (11) if $\nu = \pm 1$.

REFERENCES

[1] J. A. Buck, *Fundamentals of Optical Fibers*. New York, NY, USA: Wiley, 2004, Chs. 3 and 6.

[2] G. P. Agrawal, *Fiber-Optic Communication Systems*. New York, NY, USA: Wiley, 2011, Ch. 2.

[3] M. Brehler, M. Patchou, and P. M. Krummrich, "Impact of the refractive index profile on nonlinear effects in multimode fibers," in *Proc. ITG Symp. Photon. Netw.*, Leipzig, Germany, 2015, pp. 1–5.

[4] X. Daxhelet, L. Martineau, and J. Bures, "Influence of the fiber index profile on vectorial fiber modes and application to tapered fiber devices," *J. Lightw. Technol.*, vol. 23, no. 5, pp. 1874–1880, May 2005.

[5] K. Z. Aghaie, V. Dangui, M. J. F. Digonnet, S. Fan, and G. S. Kino, "Classification of the core modes of Hollow-Core photonic-bandgap fibers," *IEEE J. Quantum Electron.*, vol. 45, no. 9, pp. 1192–1200, Sep. 2009.

[6] A. W. Snyder and J. Love, *Optical Waveguide Theory.* New York, NY, USA: Springer, 1983, Ch. 12.

[7] M. J. Adams, *An Introduction to Optical Waveguides*. New York, NY, USA: Wiley, 1981, Ch. 7.

[8] K. Okamoto, *Fundamentals of Optical Waveguides*, 2nd ed. Burlington, NJ, USA: Academic, 2006, Ch. 3.

[9] C. L. Chen, "Excitation of higher order modes in optical fibers with parabolic index profile," *Appl. Opt.*, vol. 27, pp. 2353–2356, 1988.

[10] X. Peng *et al.*, "Higher-order mode fiber enables high energy chirped-pulse amplification," *Opt. Express*, vol. 21, pp. 32411–32416, 2013.

[11] P. Steinvurzel, J. Demas, B. Tai, Y. Chen, L. Yan, and S. Ramachandran, "Broadband parametric wavelength conversion at 1 μm with large mode area fibers," *Opt. Lett.*, vol. 39, pp. 743–746, 2014.

[12] J. Demas, P. Steinvurzel, B. Tai, L. Rishøj, Y. Chen, and S. Ramachandran, "Intermodal nonlinear mixing with Bessel beams in optical fiber," *Optica*, vol. 2, pp. 14–17, 2015.

[13] L. Rishøj, G. Prabhakar, J. Demas, and S. Ramachandran, "30 nJ, 50 fs All-Fiber Source at 1300 nm Using Soliton Shifting in LMA HOM Fiber," in *Proc. Conf. Lasers Electro-Optics*, 2016, pp. 1–2.

[14] S. Ramachandran, J. M. Fini, M. Mermelstein, J. W. Nicholson, S. Ghalmi, and M. F. Yan, "Ultra-large effective-area, higher-order mode fibers: a new strategy for high-power lasers," *Laser Photon. Rev.*, vol. 2, pp. 429–448, 2008.

[15] S. M. Israelsen, L. S. Rishøj, and K. Rottwitt, "Break up of the azimuthal symmetry of higher order fiber modes," *Opt. Express*, vol. 22, no. 10, pp. 11861–11868, 2014.

[16] E. Snitzer, "Cylindrical dielectric waveguide modes," *J. Opt. Soc. Amer.*, vol. 51, pp. 491–498, 1961.

[17] A. W. Snyder, "Excitation and Scattering of Modes on a Dielectric or Optical Fiber," *IEEE Trans. Microw. Theory Techn.*, vol. 17, no. 12, pp. 1138–1144, Dec. 1969.

Authors' biographies not available at the time of publication.